PRAMANA
— journal of
physics

Vol. 73, No. 4
October 2009
pp. 699–710

Structures, energetics and magnetic properties of $(NiSn)_n$ clusters with $n = 1$–6

V H SHEWALE[1,*], M D DESHPANDE[1] and D G KANHERE[2]
[1]Department of Physics, H.P.T. Arts and R.Y.K. Science College, Nasik 422 005, India
[2]Department of Physics and Centre for Modeling and Simulation, University of Pune, Pune 411 007, India
[*]Corresponding author. E-mail: vasundhara.aher@gmail.com

MS received 11 December 2008; revised 12 May 2009; accepted 11 June 2009

Abstract. We report the results of calculations which were performed to investigate equilibrium structures, electronic and magnetic properties of stoichiometric $(NiSn)_n$ clusters with $n = 1$–6 within the framework of density functional theory. The calculated results show that the structural arrangement of $(NiSn)_n$ clusters is dominated by the Ni–Sn and Ni–Ni interactions. We find that these binary clusters show significant variation in the geometries as compared to that of the host nickel clusters. The preference for tetrahedron unit of Ni_3Sn is seen in the lowest-energy configuration of these clusters. The multi-centre bonding between Ni atoms play an important role in stabilizing the stoichiometric Ni–Sn clusters. Doping of Sn atoms enhances the binding energy and reduces the ionization potential of nickel clusters. These binary clusters prefer the lowest spin state. For $(NiSn)_6$ the magnetic moment is 0 μB. The complete quenching of the cluster magnetic moment appears to be due to the antiferromagnetic alignment of atomic spins as revealed by the spin density plots.

Keywords. Density functional theory; bimetallic clusters; $(NiSn)_n$ clusters.

PACS Nos 31.15.Ar; 31.15.es; 31.15.xv; 36.40.Qv

1. Introduction

The research in the field of bimetallic clusters are exciting due to their potential applications in the automobile industry and hydrocarbon reactions as catalysts [1,2]. Such nanoscale alloys may present a number of structures and phases that are different from those of the corresponding pure metals. Previously, there were intensive studies on homogeneous metallic clusters [3–5]. But the reports on the bimetallic clusters are scarce, especially for transition-metal bimetallic clusters because of the complexity in their electronic structure.

Ni–Sn system forms an important class of intermetallic compounds (IMCs) with high oxidation and corrosion resistance. Huber *et al* [6] discovered a heterogeneous catalyst based on Ni, Sn and Al which is useful for various hydrocarbon reactions.

A significant amount of experimental and theoretical studies on the deposition of tin on the nickel surfaces have been conducted due to its importance in electronics and catalytic processes [7–15]. The formation of surface alloys seem to be very important in the chemical behaviour of the bimetallic catalyst. It is found that, Sn–Ni(1 1 0)c(2 × 2) surface alloy is energetically the most favourable where Sn atoms substitute Ni atoms in the outermost layers [15]. The surface studies show that Ni_3Sn_2, Ni_3Sn_4, Ni_3Sn and NiSn are the phases observed for Ni–Sn [6,7,13,14]. The binary clusters of nickel and tin atoms are expected to provide useful prototype models to understand the physics and chemistry of surfaces and nanostructures. Recently, we have initiated a systematic study of the evolution of the structural and electronic properties of small Ni–Sn clusters. Our initial study [16] on neutral and ionized small Ni_nSn ($n = 1, 12$) clusters reported their equilibrium structure, electronic and magnetic properties. The present study now proceeds to the next level of calculations on the stoichiometric $(NiSn)_n$ clusters, with $n = 1$–6. Our aim is to study how the structural properties vary with the composition and how the magnetic properties of such clusters are modified with the increase in Ni–Sn content. Specifically, we will focus on the equilibrium structure, stability, magnetization and ionization potential of stoichiometric Ni–Sn clusters using density functional theory.

The rest of the paper is organized as follows: The computational method used in this work will be presented in §2. In §3, we present the results for the ground state of the neutral and ionic clusters. In §4, conclusions will be given.

2. Computational details

All the calculations have been performed using spin density functional theory (DFT), within the ultrasoft pseudopotential plane-wave method. We have used the projector augmented wave (PAW) method [17,18] and two-parametrization for the exchange-correlation functional: the LSD approximation of Vosko *et al* [19] (VWN) and generalized gradient approximation (GGA) given by Perdew–Wang [20] as implemented in the VASP package [21]. The clusters were placed in a cubic supercell with an edge of 20 Å and periodic boundary conditions were imposed. The cut-off energy for the plane-wave was set to 269.56 eV. The optimized geometries of the clusters were obtained by quenching the various planar and three-dimensional (3D) configurations using quasi-Newton–Raphson method [21]. The structures were considered to be converged when the force on each ion was less than 0.01 eV/Å with a convergence in the total energy of about 10^{-4} to 10^{-6} eV. In all cases, the lowest-energy structure has been confirmed by changing the positions of Ni and Sn atoms, as well as by considering the configurations of the Ni clusters available from the previous studies [16,22–28]. The equilibrium geometries of the stable neutral clusters are considered as a starting point for the geometry optimization of the ionized aggregates. The stability of the lowest-energy configuration and the isomers of a given cluster is further checked by performing calculations with different spin states.

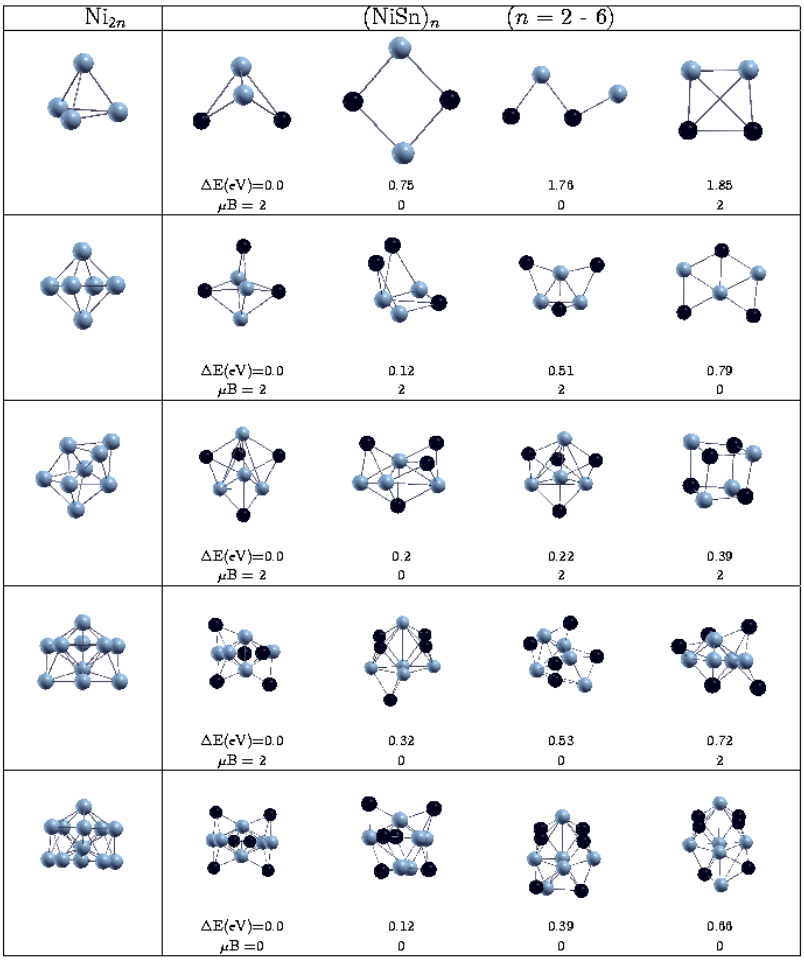

Figure 1. The ground-state geometries of Ni_{2n} clusters [16] (column 1). The structures on the right side show the lowest-energy structure (column 2) and some of the low-lying configurations for $(NiSn)_n$ clusters (n = 2–6). The lightly shaded spheres represent the Ni atoms and the dark spheres represent the Sn atoms.

3. Results

In this section, we present the equilibrium structures, stability, energetics and the magnetic moments of the $(NiSn)_n$ clusters (n = 1–6). First, we discuss the evolutionary trend of the lowest-energy structures along with some low-lying configurations. The equilibrium structures along with the host Ni_{2n} geometries are shown in figure 1. Before beginning our discussion, we note that the binding energy (BE) of Ni–Sn dimer (1.87 eV/atom) is larger than Ni_2 (1.48 eV/atom) and Sn_2 (1.65 eV/atom). The dimer bond lengths of Ni–Sn, Ni–Ni and Sn–Sn are 2.27, 2.09 and 2.78 Å respectively.

The lowest-energy configuration of $(NiSn)_2$ is a three-dimensional (3D) distorted tetrahedral structure similar to that of Ni_4. The Ni–Sn, Ni–Ni and Sn–Sn distances for tetrahedron configuration are 2.48, 2.29 and 2.95 Å respectively. The planar rhombus configuration is 0.75 eV higher in energy than the lowest 3D configuration with Ni–Sn, Ni–Ni and Sn–Sn distances 2.43, 3.62, 3.27Å respectively. The other two zig-zag and square configurations with Sn–Sn interactions are well above the lowest-energy configuration ($\Delta E = 1.76$ and 1.85 eV respectively). For zig-zag configuration Sn–Sn distance is 2.85 Å and for square configuration, it is 2.56 Å which is smaller than for Sn_2 dimer. By preferring 3D configuration $(NiSn)_2$ maximizes the overall number of bonds for both Ni–Sn and Ni–Ni as compared to that of the other planar configurations.

The lowest energy structure of $(NiSn)_3$ is the distorted octahedron configuration where two Sn atoms are bonded to three Ni atoms in a triangular pyramid configuration while one of the Sn atom is bonded to the edge of Ni_3 triangle. Three Ni atoms form the isosceles triangle with Ni–Ni distances 2.48 Å and 3.09 Å, respectively. Bi-capped rhombus configuration is one of the low-lying structure at a slightly higher energy (0.12 eV). Two Sn atoms form capping position at the two edges of Ni_3Sn rhombus. The Ni–Ni distances are 2.40 and 4.18 Å. The capped tetrahedron and planar configurations of $(NiSn)_3$ are the other low-lying structures at higher energy 0.51 and 0.79 eV, respectively. For the distorted octahedron configuration, the average coordination number for Sn atom is 2.66 while for other low-lying configurations the coordination number decreases to 2.33. Overall decrease in the coordination of Sn atoms reduces the Ni–Sn interactions which results in less stable configurations. To focus on the stability of lowest-energy configuration, we have examined the isodensity surfaces of the molecular orbitals of distorted octahedron and bi-capped rhombus configuration, a strong localization region is identified at the centre of the three Ni atoms, indicating three-centred bonding region (not shown). This is consistent with our previous result [16]. Three-centred bonding between Ni atoms stabilizes tetrahedron configuration of Ni_3Sn as compared to the rhombus structure.

Addition of one more NiSn to $(NiSn)_3$ distort the octahedron configuration significantly. The lowest-energy structure of $(NiSn)_4$ is a distorted star configuration with the central tetrahedron of Ni_4 surrounded by four Sn atoms. For each Sn atom the coordination number is three. This structure has no Sn–Sn bonds. The capped octahedron configuration is 0.2 eV higher in energy as compared to that of lowest-energy configuration. The average coordination of Sn atoms reduces to 2.75. The next low-lying configuration is 0.22 eV higher in energy, and has the same symmetry as that of the lowest-energy structure. For the lowest-energy configuration, the average Ni–Sn and Ni–Ni distances are 2.53, 2.92 Å. On the other hand, this low-lying configuration shows the respective distances to be 2.51 and 3.03 Å. This clearly indicates that the lowest-energy configuration obtained by our calculations is the result of a delicate balance between the Ni–Ni and Ni–Sn interactions. The cubic configuration is 0.39 eV higher in energy when compared to that of the lowest-energy configuration where Ni–Ni distance is 3.78 Å.

$(NiSn)_5$ is a capped pentagonal bi-pyramidal configuration. Four Sn atoms are at the capping position of each Ni_3 triangle and one of the Sn atom caps at the edge of the Ni_3 triangle having coordination number two. The capped triangular

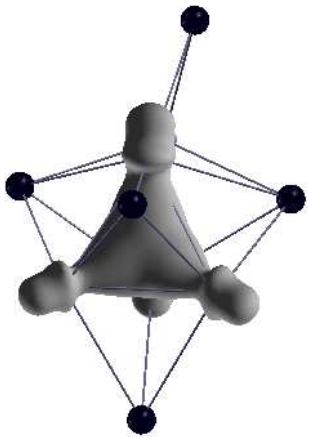

Figure 2. Isodensity surface corresponding to the HOMO-30 state for the lowest-energy configuration of $(NiSn)_5$, at one-fifth of its maximum isosurface value.

pyramid configuration is found to be one of the low-lying structures (0.32 eV) where the average coordination number for all Sn atoms is three. To focus on the stability of lowest-energy configuration, we have examined the molecular isodensity isosurfaces of the molecular orbitals of lowest and low-lying structures. In our discussion a typical occupied orbital is denoted by the notation HOMO-n, where n represents the number of levels counted from HOMO (highest occupied molecular orbital). Figure 2 shows the isodensity surface for HOMO-30 of the lowest-energy configuration, a strong localized region is identified at the centre of the tetrahedron of Ni_4 indicating the multi-centred bonding region. This makes capped pentagonal bi-pyramidal structure more stable when compared to that of the other low-lying configurations.

$(NiSn)_6$ can be viewed as an octahedron of Ni_6 surrounded by six Sn atoms. The central ring consists of four Ni and two Sn atoms. The distorted capped pentagonal bi-pyramidal configuration is 0.12 eV higher in energy than the six-membered bi-pyramidal capped configuration. The capped octahedron with different capping positions of Sn atoms are the other low-lying configurations (0.39 eV and 0.66 eV respectively).

The overall evolutionary trend for $(NiSn)_n$ series shows that, the Sn atom prefers to maximize Ni–Sn bonds by selecting the tetrahedral site which increases the coordination of Ni atoms with Sn atoms. Tin atoms induce significant distortion in the geometries of the nickel cluster. The preference for tetrahedron unit of Ni_3Sn is seen in the lowest-energy configuration of these clusters. The lowest-energy configuration does not have Sn–Sn bonds. These structural trend can be explained on the basis of the electronic structure of the cluster which will be discussed in the next section.

All the ground state configurations of anionic and cationic $(NiSn)_n$ clusters ($n \leq 6$) (not shown) are similar to that of neutral configurations. It is also found that, when the cation is formed, the Ni–Sn bond lengths increase with respect to the neutral cluster while the addition of electron enhances the Ni–Sn interactions by

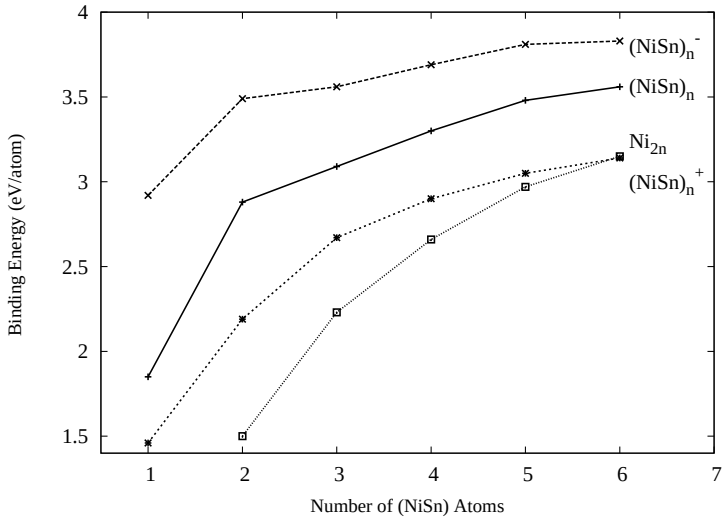

Figure 3. Binding energy per atom (eV) for neutral, ionic $(NiSn)_n$ (n = 1–6) and Ni_{2n} [16] clusters vs. number of (NiSn) atoms in the cluster.

decreasing the Ni–Sn bond lengths. This is consistent with the previous results [16]. The stability of neutral and ionic clusters can be found by calculating the binding energy per atom (E_b).

The binding energy (BE) is calculated as

$$E_b[(NiSn)_n] = [-E[(NiSn)_n] + nE[Ni] + nE[Sn]]/2n, \quad (1)$$

where E is the total energy of the system.

The binding energy per atom (in eV) for $(NiSn)_n$ neutral and ionic clusters against the number of (NiSn) atoms is shown in figure 3. For comparison, we have also plotted the binding energy per atom (in eV) for Ni_{2n} cluster, which clearly indicates that the substitution of the Ni atom by Sn enhances the binding energy of the given cluster. With the increase in the number of NiSn units (n = 2–6), the average coordination number of Sn atoms with Ni increases from 2, 2.66, 3, 3.2, 3.33. The increase in the coordination number of Sn atoms with Ni increases the binding energy of the cluster. The BE curves for anionic and cationic clusters show similar nature as that of the neutral clusters. As noted earlier, the addition of an electron increases the Ni–Sn interaction by decreasing the Ni–Sn bond lengths in anionic clusters. This will enhance the binding energy of $(NiSn)_n^-$ as compared to neutral one as well as the host clusters. But the removal of electron decreases the Ni–Sn interaction which results in less stability for the cationic clusters.

To evaluate the relative stability of these clusters, it is more meaningful to calculate the energy gain in adding a NiSn molecule to the preceding cluster, namely $\Delta E = E(NiSn)_n - (E(NiSn)_{n-1} + E(NiSn))$. For n = 2–6, the ΔE values are 4.02, 3.27, 4.12, 4.58 and 4.16 eV, respectively. This shows that $(NiSn)_3$ is relatively unstable with respect to dissociation. In going from $(NiSn)_2$ to $(NiSn)_3$ the average bond distance R_{Ni-Sn} increases by 2% and decreases by 1% from $(NiSn)_3$ to

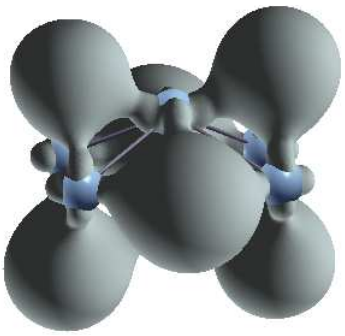

Figure 4. Isodensity surface corresponding to the HOMO-35 state for the lowest-energy configuration of $(NiSn)_6$, at one-fifth of its maximum isosurface value.

$(NiSn)_4$. Even though the average coordination of Sn atoms increases as compared to $(NiSn)_2$ cluster, the decrease in Ni–Sn interactions makes the cluster relatively unstable. Similarly, in going from $(NiSn)_5$ to $(NiSn)_6$, the R_{Ni-Sn} distance increases by 1%.

To discuss the nature of the bonding in these clusters, we have examined the charge density isosurfaces of the molecular orbitals and the eigenvalue spectrum (not shown) for the lowest and some of the low-lying configurations of all clusters. The localized charge density distribution is found around Ni atoms. The charge transfer is observed from Sn to Ni. The HOMO of all the lowest-energy configurations belongs to Ni-d. The hybridized Sn_p–Ni_d states are at the middle of the energy spectrum. A typical state from the lowest-energy configuration of $(NiSn)_6$ is shown in figure 4. It is seen that Sn-p is hybridized with Ni-$d_{x^2-y^2}$. The relative bonding between Sn atoms is weak and stability of these clusters could be enhanced by prompting Ni–Sn and Ni–Ni bonds.

Now we discuss the nature of the HOMO for the lowest-energy configuration of all the clusters. With the increase in n, the subsequent addition of NiSn unit induces the hybridized states at the middle of the energy spectrum and the localized d orbitals are found at HOMO or near HOMO. Figures 5 and 6 show the isodensity surfaces for the HOMO of $(NiSn)_5$ and $(NiSn)_6$ clusters. It is seen that, for $(NiSn)_6$ the HOMO (figure 6) is dominated by $d_{x^2-y^2}$ while for $(NiSn)_5$ (figure 5), a mixture of $d_{x^2-y^2}$ and d_{z^2} is observed on the Ni atoms. For the lowest-energy configuration of $(NiSn)_6$, all Sn atoms are at the tetrahedral position while for $(NiSn)_5$, one of the Sn atom is with the coordination number two. The decrease in Ni–Sn interaction induces a mixture of more number of Ni_d states near HOMO which leads to the inhomogeneous distribution of charge density. For $n \leq 5$ the preferred spin state is two while for $(NiSn)_6$ the spin state is zero.

The total magnetic moment for $(NiSn)_n$ clusters against the number of atoms in the cluster is shown in figure 7, where we have also plotted total moment of the host nickel clusters. It is seen that the doping of the Sn atom reduces the magnetic moment of the nickel clusters significantly. All the lowest-energy and low-lying configurations of $(NiSn)_n$ clusters prefer the spin state either 0 or 2. The total magnetic moment of Ni–Sn diatomic system is 0 μB. For n = 2–5, the clusters have

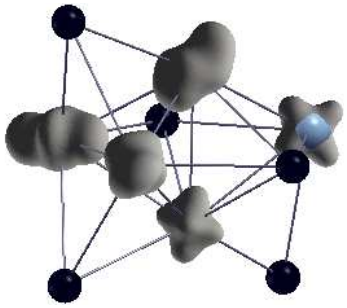

Figure 5. Isodensity surface corresponding to the HOMO state for the lowest-energy configuration of $(NiSn)_5$ at one-fifth of its maximum isosurface value.

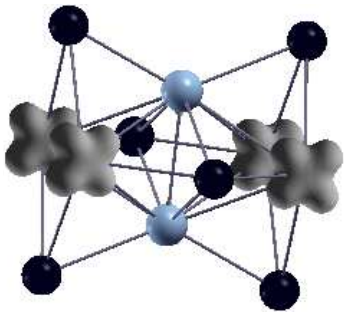

Figure 6. Isodensity surface corresponding to the HOMO state for the lowest-energy configuration of $(NiSn)_6$ at one-fifth of its maximum isosurface value.

the magnetic moment $2\,\mu$B while for $(NiSn)_6$, it is $0\,\mu$B. The spin state of the cluster appears to depend on the coordination of Sn atoms, Ni–Ni distances, the nature of hybridization of Ni-d with Sn-p, and cluster symmetry. For example, the magnetic moment for the tetrahedron unit of $(NiSn)_2$ is $2\,\mu$B, while for the planar rhombus configuration it is $0\,\mu$B. The increase in Ni–Sn interactions reduces the magnetic moment to 0 μB. It is already noted that for $n \leq 5$, some of the Sn atoms are not at the tetrahedron site. The reduced coordination number of Sn atoms results in the inhomogeneous distribution of the Ni-d orbitals near HOMO. The consequence of this is leading to the enhancement in the magnetic moment to $2\,\mu$B.

The calculated total density of states (DOS) further provides an explanation of the magnetic behaviour of these clusters (figure 8). The Fermi level passes through the Ni-d level for the majority spin, thereby confirming the contribution from the Ni-d orbitals to the net magnetic moment. The hybridized Ni_d–Sn_p states are found at the middle of the spectrum. Successive addition of NiSn leads to the broadening of the majority and minority spins. The subsequent addition of Ni–Sn unit increases the degree of hybridization leading to the shift of the majority and minority spins below Fermi level. For $(NiSn)_2$ to $(NiSn)_5$, the projected DOS on Ni atoms shows the delocalized spin-down states as compared to the spin-up states. The major contribution to the magnetic moment is now from the minority spin. On the other

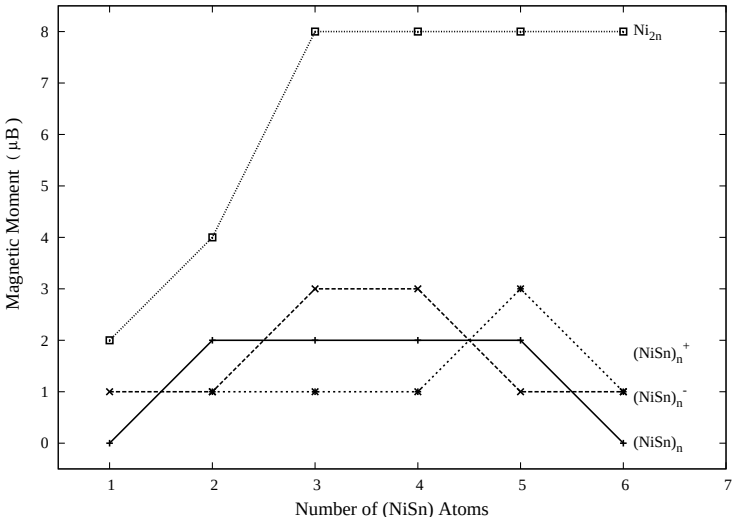

Figure 7. Total magnetic moment (in μB) for the neutral, ionic $(NiSn)_n$ (n = 1–6) and the Ni_{2n} [16] structures as a function of the number of (NiSn) atoms in the cluster.

hand, at $(NiSn)_6$, the projected DOS on Ni atoms shows symmetric majority and minority states suggesting the system to be non-magnetic. Overall, the transition from ferromagnetic to antiferromagnetic ordering therefore quenches the magnetic moment of the cluster.

In this paper, we provide a systematic study of the adiabatic electron affinity (EA) and the ionization potential (IP). Adiabatic electron affinity (AEA) is defined as the energy difference between the anionic and neutral clusters at their own respective optimized geometries. While the adiabatic ionization potential (AIP) is defined as the energy difference between the cationic and neutral clusters at their own respective optimized geometries, vertical electron affinity (VEA) is defined as the energy difference between the anionic and neutral clusters with both at the optimized geometry of the anionic cluster. The vertical ionization potential (VIP) is defined as the energy difference between the cationic and neutral clusters with both at the optimized geometry of the neutral cluster.

Table 1 shows the calculated ionization potential (IP) and the electron affinity (EA) of the $(NiSn)_n$ clusters. The IPs show slight decrease from NiSn to $(NiSn)_6$ while EAs increase with n. The vertical and adiabatic EAs and IPs are nearly the same which indicate that there is not much topological differences between neutral and ionic configurations of $(NiSn)_n$ clusters. For comparison, we have also noted their results for vertical ionization potential of nickel clusters. It clearly indicates that the doping with Sn atom reduces the ionization potential of nickel clusters.

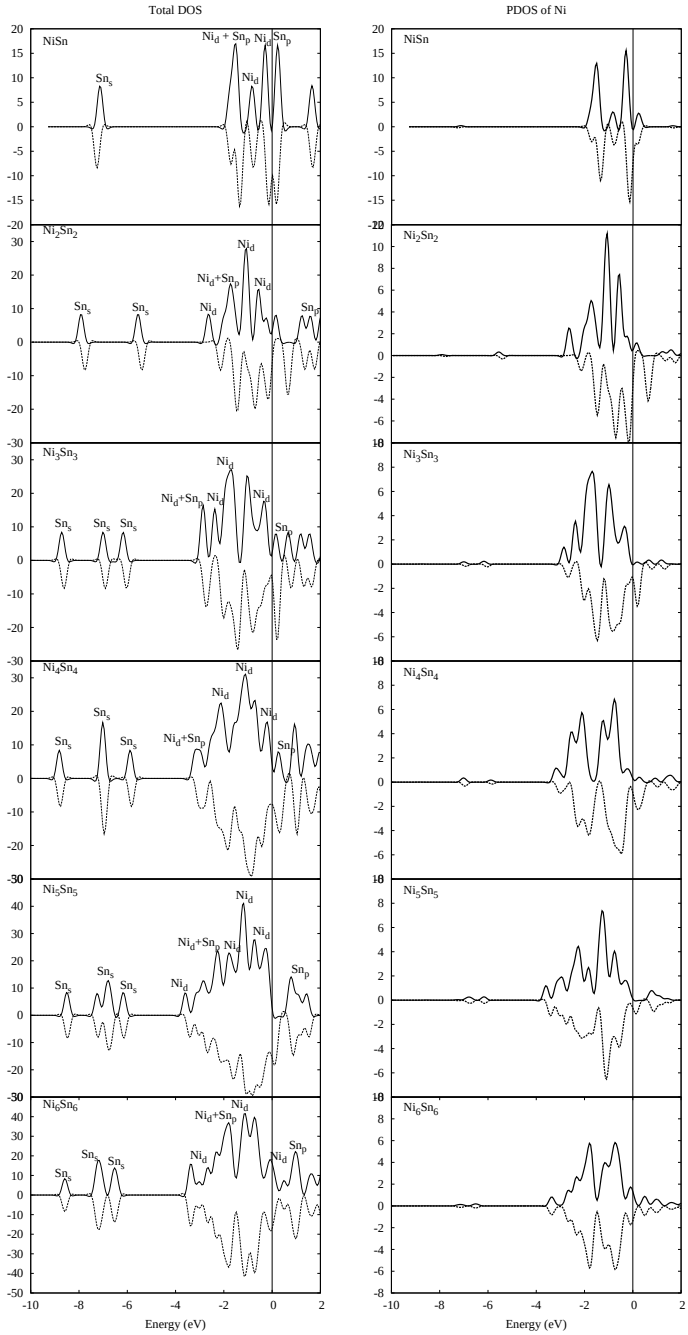

Figure 8. Total density of states (DOS) and partial DOS associated with Ni atoms for $(NiSn)_n$, $n = 1$–6. The Fermi level given by the dotted line is aligned to zero.

Table 1. Adiabatic and vertical values (eV) of the ionization potential and electron affinity for $(NiSn)_n$ clusters (n = 1–6) along with vertical ionization potential of Ni_{2n} cluster [25].

	n =					
System	1	2	3	4	5	6
VIP-Ni_{2n}	8.30	5.90	6.80	6.50	6.20	6.10
AIP	–	5.54	5.17	5.11	5.09	4.90
VIP	–	5.59	5.23	5.14	5.12	4.91
AEA	2.08	2.43	2.80	3.10	3.33	3.33
VEA	2.06	2.43	2.75	3.04	3.32	3.32

4. Conclusions

In the present investigation, we have reported the lowest-energy and some of the low-lying configurations of $(NiSn)_n$ (n = 1–6) using density functional theory. The overall evolutionary trend shows that, the substitution of Ni by Sn distorts the host geometries significantly where the Sn atom occupies the tetrahedral site in the cluster. The doping of Sn atoms enhances the binding energy, reduces the magnetic moment and the ionization potential of the nickel cluster. For stoichiometric $(NiSn)_n$ clusters, the structural stability and magnetic properties appear to be the outcome of a delicate interplay among the coordination number of Sn atom, cluster symmetry and the hybridization of Sn-p and Ni-d orbitals. All the clusters prefer lowest spin state. The decrease in the cluster magnetic moment is attributed to the antiferromagnetic alignment of small individual atomic moments arising due to the hybridization of Ni-d and Sn-p orbitals in the cluster.

Acknowledgements

The author gratefully acknowledge the Centre for Simulation and Modeling and Department of Physics, University of Pune, India for allowing us to use their computing facility. MDD acknowledges partial financial assistance from the University Grants Commission and University of Pune, India.

References

[1] J H Sinfelt, *Bimetallic catalysts*: *Discoveries, concepts and applications* (Wiley, New York, 1983)
[2] K C Taylor, *Automobile catalytic converters* (Spinger, New York, 1984)
[3] V Kumar, K Esfarjani and Y Kawazoe, Springer series in cluster physics in: *Clusters and nanomaterials* (Springer-Verlag, Berlin Heidelberg, 2002)
[4] *Clusters and nanostructured materials* edited by P Jena and S N Behera (Nova Science Publishers, Inc., New York, 1996)
[5] J A Alonso, *Chem. Rev.* **100**, 637 (2000)

[6] G W Huber, J W Shabaker and J A Dumesic, *Science* **300**, 2075 (2003)
[7] A Onda, T Komatsu and T Yashima, *Phys. Chem. Chem. Phys.* **2**, 2999 (2000)
[8] Tuan-Chi Liu and Shwu-Jer Chiu, *Ind. Eng. Chem. Res.* **33**, 488 (1994)
[9] M L Ferreira, N N Nichio and O A Ferretti, *J. Mol. Cata. A: Chem.* **202**, 197 (2003)
[10] J W Shabaker, D A Simonetti, R D Cortright and J A Dumesic, *J. Catalysis* **231**, 67 (2005)
[11] S H Overbury and Yi-sha Ku, *Phys. Rev.* **B46**, 7868 (1992)
[12] Y D Li, L Q Jiang and B E Koel, *Phys. Rev.* **B49**, 2813 (1994)
[13] M Masai, K Mori, H Muramoto, T Fujiwara and S Ohnaka, *J. Catalysis* **50**, 419 (1977)
[14] C Schmetterer, H Flandorfer, K W Richter, U Saeed, M Kauffman, P Roussel and H Ipser, *Intermetall.* **15**, 869 (2007)
[15] D F Li, H Y Xiao, X T Zu and H N Dong, *Mater. Sci. & Eng.* **A460**, 50 (2007)
[16] M D Deshpande, Swapna Roy and D G Kanhere, *Phys. Rev.* **B76**, 195423 (2007)
[17] P E Blochl, *Phys. Rev.* **B50**, 17953 (1994)
[18] G Kresse and J Furthmuller, *Phys. Rev.* **B59**, 1758 (1999)
[19] S H Vosko, K Wilk and N Nusair, *Can. J. Phys.* **58**, 1200 (1980)
[20] J P Perdew and Y Wang, *Phys. Rev.* **B45**, 13244 (1992)
[21] Vienna *ab initio* Simulation Package (VASP), Technische Universität Wien (1999)
[22] F A Reuse and S N Khanna, *Chem. Phys. Lett.* **234**, 77 (1995)
[23] F A Reuse, S N Khanna and S Bernel, *Phys. Rev.* **B52**, R11650 (1995)
[24] S K Nayak, S N Khanna, B K Rao and P Jena, *J. Phys. Chem.* **A101**, 1072 (1997)
[25] B V Reddy, S K Nayak, S N Khanna, B K Rao and P Jena, *J. Phys. Chem.* **A102**, 1748 (1998)
[26] S N Khanna, M Beltran and P Jena, *Phys. Rev.* **B64**, 235419 (2001)
[27] M Moskovits and J E Hulse, *J. Chem. Phys.* **66**, 3988 (1977)
[28] E K Parks, L Zhu, J Ho and S J Riley, *J. Chem. Phys.* **100**, 7206 (1994); *J. Chem. Phys.* **102**, 7377 (1995)